Check for updates

physica status solidi a
www.pss-a.com

Signatures of Mesoscopic Transport in Single Non-Intentionally Doped GaN-Nanowire Field-Effect Transistors

Hannes Hergert, Mario F. Zscherp, Philip Klement, Jörg Schörmann, Sangam Chatterjee, Peter J. Klar, and Matthias T. Elm*

In this work, the fabrication and characterization of a fully functional field-effect transistor (FET) are addressed based on a non-intentionally doped GaN-nanowire FET (NW–FET). Universal conductance fluctuations (UCFs) are observed at temperatures below 140 K. In contrast to other reports in literature, UCFs appear in the analyzed NW–FET only under the influence of an electrical field when applying a gate voltage, while no UCF signatures are observed when performing magnetic-field-dependent measurements. The reason is the considerable impact of the applied voltage on the narrow conductive channel of the non-intentionally doped NW. The electrical field influences the Fermi level as well as the width of the depletion region, both changing the effective impurity distribution which determines the set of possible electron paths. The electric-field-induced variation of the set of electron paths correlates with a conductance variation, which leads to the occurrence of UCFs. Furthermore, the reliability of determining the phase coherence length l_ϕ from the NW–FET transfer characteristics is analyzed. It is shown that the value of l_ϕ is significantly affected by the choice of the gate voltage range due to the current dependence of the magnitude of the UCFs.

1. Introduction

The III–V semiconductors are widely used as functional material for all kinds of optoelectronic applications such as gas sensors, light-emitting diodes, and field-effect transistors (FETs).[1–10] Especially gallium nitride (GaN) nanowires (NWs) are of vast interest for high temperature and high-power switching devices.[10–19] In addition to their wide and direct bandgap, GaN NWs stand out due to their quasi one-dimensionality which enables the exploration of low-dimensional transport phenomena.[20–23] One prominent example of such transport phenomena on the mesoscopic scale are universal conductance fluctuations (UCFs). UCFs arise in low-dimensional nanostructures due to the quantum mechanical interference of different electron paths.[24] The interference of those paths is only possible if the electron wave functions are coherent. This means that the phase coherence length l_ϕ, which describes the characteristic length over which the electron phase is maintained, needs to be comparable or larger than the characteristic dimensions (diameter, length) of the NW.[24] Once the electron paths are manipulated either by a magnetic or an electric field, fluctuations of the electron conductivity of the system arise as a result of the interference effects. Inelastic scattering events become more important with increasing temperature resulting in a decrease of the phase coherence length. Consequently, the quantum interference effects vanish due to thermal averaging, and the phase coherence length reveals a characteristic temperature dependence as a function of the dominant scattering mechanism and the effective quasi-dimensionality of the system.[25,26] Thus, the analysis of the phase coherence length in mesoscopic systems, such as NWs, is a powerful tool to identify the underlying scattering mechanisms.

In contrast to many other works, where UCFs in GaN NWs are identified by measuring the conductance for varying magnetic field (magnetic field approach), we are able to induce UCFs in a non-intentionally doped NW–FET by applying a gate voltage instead (electric field approach).[22,23,25,27–30] The analysis of the magnitude of the conductance fluctuations reveals a phase coherence length of about 10 nm, which is in excellent

H. Hergert, M. F. Zscherp, P. Klement, J. Schörmann, S. Chatterjee, P. J. Klar
Center for Materials Research
Institute of Experimental Physics I
Justus Liebig University Giessen
Giessen 35392, Germany
E-mail: hannes.hergert@physik.uni-giessen.de

M. T. Elm
Center for Materials Research
Institute of Experimental Physics I
Institute of Physical Chemistry
Justus Liebig University Giessen
Giessen 35392, Germany

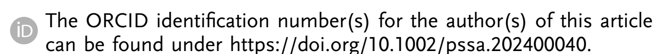
The ORCID identification number(s) for the author(s) of this article can be found under https://doi.org/10.1002/pssa.202400040.

© 2024 The Authors. physica status solidi (a) applications and materials science published by Wiley-VCH GmbH. This is an open access article under the terms of the Creative Commons Attribution-NonCommercial License, which permits use, distribution and reproduction in any medium, provided the original work is properly cited and is not used for commercial purposes.

DOI: 10.1002/pssa.202400040

agreement with previously reported values obtained from the analysis of the weak localization effect.[25] Our results show that the electrical field approach is well suited for determining the phase coherence length in non-intentionally doped NWs, which will help to obtain a better fundamental understanding of dominant scattering mechanisms in these low-dimensional systems.

2. Experimental Section

2.1. Devices Fabrication

2.1.1. NW Growth

Non-intentionally doped GaN NWs were grown on Si(111) substrates using plasma-assisted molecular-beam epitaxy as reported in detail in literature.[31] Real-time structural analysis of the growing NWs was facilitated by reflection high-energy electron diffraction (RHEED). Prior to the NW growth, the substrate was heated to 820 °C at a chamber pressure of 10^{-9} mbar for a few minutes, before reducing the temperature back to 780 °C. This process induced a clean Si-7 × 7 surface reconstruction, confirmed by RHEED analysis. Subsequently, the silicon surface was nitrided under nitrogen flow of 0.8 sccm and plasma power of 400 W to create an amorphous silicon nitride surface. The wire growth took place at 780 °C under nitrogen-rich conditions with a plasma power of 300 W and nitrogen flow of 1 sccm, corresponding to a partial pressure of 1.7×10^{-5} mbar. The gallium effusion cell was heated to 910 °C resulting in a beam equivalent pressure of 1.5×10^{-7} mbar. These growth conditions yield a n-type carrier concentration of about 10^{19} cm^{-3}, which arises due to Si diffusion from the substrate into the NW during growth as well as oxygen impurities as discussed in more detail in our previous publication.[32] After a growth period of 5 h, the apertures of the effusion cell and the plasma source were closed, terminating the wire growth. This growth process yielded a multitude of homogeneous NWs which were 40–100 nm thick and about 2 μm long.

2.1.2. NW–FET Fabrication

The fabrication of single NW–FETs was realized following the standard recipe described in our previous work.[25,27,32,33] First NWs were transferred onto a Si/SiO_2 chip and localized by scanning electron microscope (SEM). Individual electrical contacts for the single NWs were transferred onto the chip by a combination of photo- and electron-beam lithography (EBL). Metal layers, Ni (20 nm) and Au (200 nm), were deposited by electron-beam physical vapor deposition to form the contact leads. Ohmic contacts of the NWs were obtained by annealing at 10^{-6} mbar for 90 s at 600 °C. For the preparation of the NW–FET structure, a 7.5 nm thick hafnium dioxide (HfO_2) insulating layer was deposited by a combination of EBL and atomic layer deposition for separating NW and the top gate. After this step, the top gate was implemented in the same manner as the NW contacts. An SEM image of the finalized NW–FET is shown in **Figure 1** alongside a sketch of the idealized NW–FET structure. The NW has a length of about 2000 nm and a diameter of 80 nm. The distance between the source and drain contacts is about 1100 nm and the gate is 530 nm wide.

2.2. Measurement Setup

The DC transport measurements were performed in an Oxford Instruments liquid-helium cryostat enabling temperature-dependent measurements between 1.7 and 270 K. Transistor measurements were conducted at gate voltages (V_G) varying between −4 and +5 V and a drain-to-source voltage (V_{DS}), varying between −30 and +30 mV using a Keithley parameter analyzer. Higher voltages were avoided to prevent damaging of the NW–FET.

3. Results and Discussion

3.1. Transport Properties

A functional NW–FET needs to fulfill two particularly important criteria in addition to its switching characteristics. One is the Ohmic behavior of the NW resistance and the other the electrically insulating behavior of the top gate in the entire temperature range of interest. The current–voltage characteristics of the NW are shown in **Figure 2**a. Slight deviations from a linear behavior occur only at negative drain–source voltage V_{DS} higher than −35 mV and below 50 K. The resistance of the NW varies from 4.2×10^5 Ω (270 K) to 5.6×10^5 Ω (1.7 K). Figure 2b shows the leakage current I_G through the top gate plotted against the gate voltage V_G, which proves an adequate insulating behavior of the HfO_2 layer. Only for temperatures above 200 K, the leakage current approaches values of about 1 nA at high gate voltages. However, this value is still negligible as it is two orders of

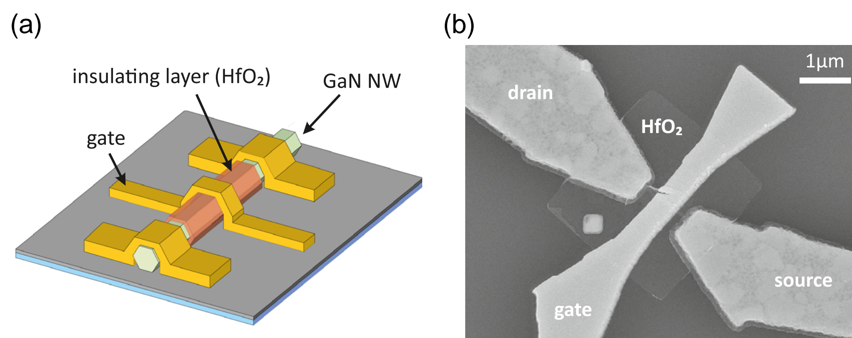

Figure 1. a) Schematic drawing of a finalized NW–FET and b) SEM image of the analyzed NW–FET.

© 2024 The Authors. physica status solidi (a) applications and materials science published by Wiley-VCH GmbH

18626319, 2024, 21, Downloaded from https://onlinelibrary.wiley.com/doi/10.1002/pssa.202400040 by Justus-Liebig-Universitat, Wiley Online Library on [27/11/2024]. See the Terms and Conditions (https://onlinelibrary.wiley.com/terms-and-conditions) on Wiley Online Library for rules of use; OA articles are governed by the applicable Creative Commons License

18626319, 2024, 21, Downloaded from https://onlinelibrary.wiley.com/doi/10.1002/pssa.202400040 by Justus-Liebig-Universitat, Wiley Online Library on [27/11/2024]. See the Terms and Conditions (https://onlinelibrary.wiley.com/terms-and-conditions) on Wiley Online Library for rules of use; OA articles are governed by the applicable Creative Commons License

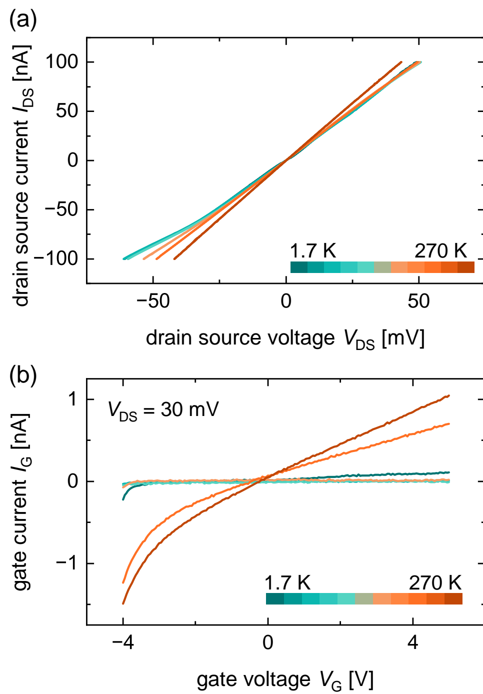

Figure 2. Current–voltage characteristics of a) the nanowire and b) the top gate in the temperature range between 1.7 and 270 K.

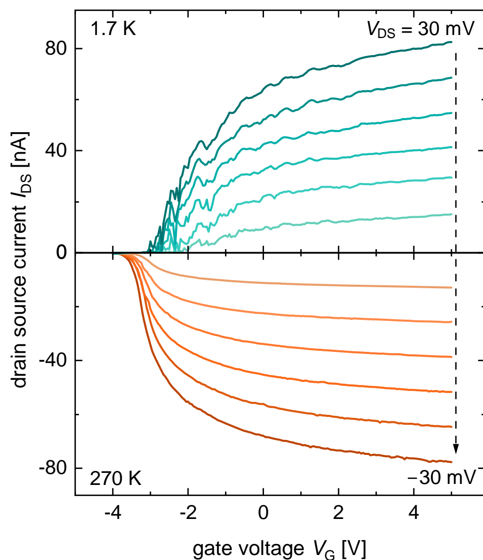

Figure 3. Transfer characteristics I_{DS} versus V_G of the NW–FET at 1.7 K (top) and 270 K (bottom) for V_{DS} varying between 5 and 30 mV and −5 to −30 mV, respectively.

magnitude lower than the drain–source current (I_{DS}) flowing through the NW itself. The average resistance of the top gate varies between $5 \times 10^9\,\Omega$ (270 K) and $1.6 \times 10^{10}\,\Omega$ (1.7 K) confirming its insulating behavior.

Figure 3 shows the transfer characteristics, i.e., the drain–source current I_{DS} plotted versus the gate voltage V_G, of the fabricated GaN-NW–FET for the lowest temperature of 1.7 K and the highest temperature of 270 K investigated. In both cases and at all temperatures in between, as shown in Figure S1, Supporting Information, the drain source current I_{DS} follows the typical behavior of a FET, i.e., the drain–source current shows a steep linear increase starting above the threshold voltage (V_{th}) followed by a saturating behavior toward higher gate voltages.[34] However, there are also some significant differences between the high- and low-temperature behavior of the transfer characteristics. For example, the threshold voltage is shifted to more negative values with increasing temperature, while UCFs are appearing at low temperatures. The temperature dependence of the threshold voltage of the GaN-NW–FET analyzed corresponds to the expected behavior of a classical metal oxide FET as it is inversely proportional to the temperature.[34] The most prominent difference between the characteristics at high and low temperatures, namely the arising UCFs, will be discussed in the following section.

3.2. Universal Conductance Fluctuations

The UCFs arise when the temperature is decreased below 140 K. The temperature dependence of the UCFs can be observed in more detail in Figure S1, Supporting Information, where only transfer curves at $V_{DS} = 30$ mV are shown for temperatures varying between 1.7 and 140 K. To separate the absolute UCFs from the transfer curve, a typical FET transfer characteristic is fitted to the measured transfer characteristics and subtracted from it. Two of the fit curves used during the analysis, one for a high and the other for a low temperature, are shown in Figure S2, Supporting Information. The absolute UCFs obtained are presented in **Figure 4**a. The stability of the fluctuation patterns for increasing temperature is a typical property of UCFs,[24] which occur due to voltage-induced changes of the possible pathways for an electron moving through the sample.[24] Furthermore, the magnitude of the conduction fluctuations decreases with increasing gate voltage V_G. This is caused by the resulting high current density in the NWs at high gate voltages, which leads to an increased number of uncorrelated energy intervals contributing to the electron transport and, thus, to current-induced averaging of the fluctuations.[27]

It is worth noting that no conductance fluctuations occur and only a weak localization effect is observed when applying a magnetic field as can be seen in Figure S3, Supporting Information. These findings are in agreement with previous results.[25] Instead, the UCFs arise for the non-intentionally doped GaN NW only when a gate voltage is applied. This can be attributed to two effects. First, the applied gate voltage shifts the Fermi level of the electrons resulting in an effective change of the impurity distribution at which the electrons can scatter. Second, the conductive channel for the freely moving electrons inside the NW is modified under the influence of an applied electrical field. Increasing the gate voltage V_G leads to a broadening of this channel. This also modifies the effective impurity distribution in the conductive channel due to additional transport paths for the electrons. In both cases, the set of possible interfering electron paths changes with varying gate voltage and, hence, the conductance fluctuates.

© 2024 The Authors. physica status solidi (a) applications and materials science published by Wiley-VCH GmbH

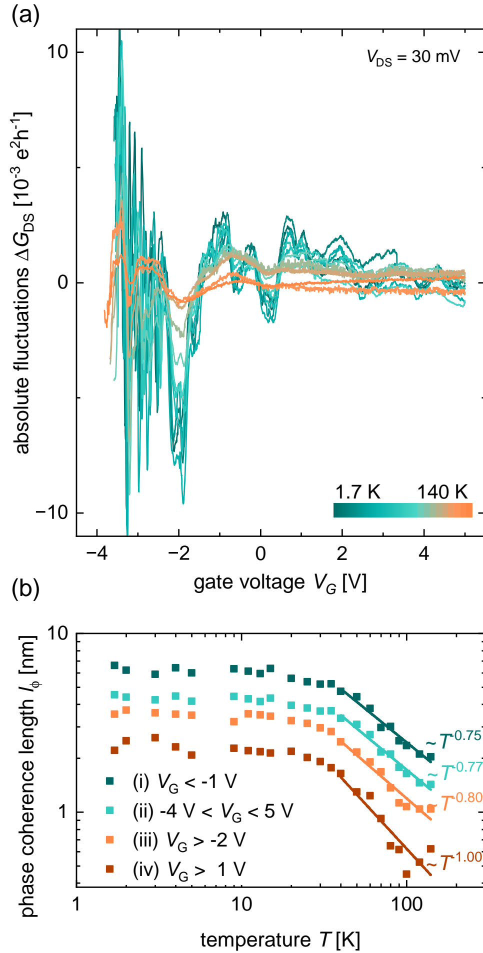

Figure 4. a) Absolute magnitude of the fluctuations ΔG at $I_{DS} = 30$ mV for temperatures between 1.7 and 140 K and b) temperature dependence of the phase coherence length l_ϕ analyzed for different V_G ranges.

Voltage-induced changes of the channel width and the Fermi level are expected to have a significant impact on the effective impurity distribution only for a narrow conductive channel with a low impurity distribution. This situation is given in case of the non-intentionally doped GaN NW investigated in this work. Its conductive channel is much smaller than the NW diameter due to an upward surface band bending.[25] The width of the resulting depletion region has been estimated to be up to 20 nm for the non-intentionally doped GaN NW, which reduces the width W of the conductive channel to about 40 nm.[25,35] When applying a positive gate voltage, the Fermi level is shifted upward reducing the width of the depletion region, and at high positive gate voltages, the whole NW serves as conductive channel. Applying a negative gate voltage reduces the width of the conductive channel by shifting the Fermi level energetically downward. At about $V_G = -2$ V, the channel is completely closed as the depletion region extends over the whole NW. The impact of the applied gate voltage on the width of the conductive channel is schematically depicted in Figure S4, Supporting Information. This may also be the reason for the absence of UCFs when applying a magnetic field as the magnetic-field induced deflection only slightly distorts the electron pathway in narrow channels. The opposite situation may be expected for NWs with a wide conductive channel, e.g., in highly doped NWs with a small depletion region. Here, the relative change of the effective impurity distribution due to an applied gate voltage can be neglected, while an external magnetic field can significantly affect the electron pathways.

Analyzing the UCF allows the determination of the phase coherence length l_ϕ as well as its temperature dependence. At finite temperatures, thermal averaging needs to be considered which is characterized by the thermal length l_T.[24,36] For $l_\phi \ll l_T$, the effect of thermal averaging is negligible, while thermal averaging results in a reduction of the fluctuation amplitude for $l_\phi \geq l_T$.[36] Typically, l_ϕ is comparable to l_T for non-intentionally doped GaN NWs. An estimation for $T = 1$ K according to literature yields $l_T = 12$ nm,[32] which is what we assume for the NW–FET investigated in this work.[22,37] Then, l_ϕ can be estimated from the mean fluctuation amplitude of the UCF with an accuracy of about 10%:

$$\mathrm{rms}(\Delta G) = \alpha \frac{e^2}{2\pi\hbar}\left(\frac{l_\phi}{L}\right)^{\frac{3}{2}}\left[1+\frac{\alpha}{\beta}\left(\frac{l_\phi}{l_T}\right)^2\right]^{-\frac{1}{2}} \tag{1}$$

with $\alpha = \sqrt{6}$, $\beta = \sqrt{4\pi/3}$ and $L = 1100$ nm being the length of the NW.[38] l_ϕ is two orders of magnitude smaller than L. Thus, statistical averaging of the fluctuations occurs, which reduces the fluctuation magnitude significantly by three orders of magnitude yielding values of $\mathrm{rms}(\Delta G) = 10^{-3}\,\mathrm{e}^2\,\mathrm{h}^{-1}$. The results clearly demonstrate the suitability of the electrical field approach even for determining phase coherence lengths of the order of a few nanometers only. It is important to note that the small-phase coherence length of only a few nanometers also explains the absence of UCFs when applying a magnetic field. To induce UCFs when applying a magnetic field, a magnetic field strength of the order of the correlation field B_C is needed:

$$B_C = \gamma \frac{\Phi_0}{l_\phi d} \tag{2}$$

where Φ_0 is the magnetic flux quantum, γ is a numerical parameter depending on the transport regime, and d is the NW diameter. The quantity $l_\phi d$ can be interpreted as the average area enclosed by phase-coherent electrons in the NW. A rough estimation using the l_ϕ values obtained from the analysis of $\mathrm{rms}(\Delta G)$ shows that magnetic fields larger than 40 T are needed to observe UCF with the magnetic field approach.

As the conductance fluctuations ΔG decrease with increasing V_G,[27] the root mean square (rms) value of the fluctuations and therefore also l_ϕ vanish at high gate voltages. In contrast, the rms value of the fluctuations is higher at low-gate voltages. However, the overall measurement current is comparatively low. This results in a non-negligible contribution of random measurement noise to the fluctuations, which may obscure the estimated value of l_ϕ when using Equation (1). Thus, it is necessary to identify the best suited voltage range for a reliable determination of l_ϕ. We analyzed the UCFs in four different voltage ranges: 1) only the negative voltage range from −4 to −1 V, 2) the entire voltage

© 2024 The Authors. physica status solidi (a) applications and materials science published by Wiley-VCH GmbH
18626319, 2024, 21, Downloaded from https://onlinelibrary.wiley.com/doi/10.1002/pssa.202400040 by Justus-Liebig-Universitat, Wiley Online Library on [27/11/2024]. See the Terms and Conditions (https://onlinelibrary.wiley.com/terms-and-conditions) on Wiley Online Library for rules of use; OA articles are governed by the applicable Creative Commons License

range from −4 to +5 V, 3) an intermediate voltage range from −2 to +5 V, and 4) the high voltage range from +1 to +5 V. The obtained temperature dependences of l_ϕ for all four voltage ranges are shown in Figure 4b. In the entire temperature range, l_ϕ differs by up to a factor of four between the highest and lowest analyzed gate voltage range. l_ϕ is largest in the low voltage range (1), as the random noise superimposes the fluctuations and, thus, results in an overestimation of l_ϕ. When only considering the high gate voltage range (4), the smallest values of l_ϕ are obtained. The apparent decrease of l_ϕ in the high gate voltage range arises from the current dependence of the fluctuation magnitude rms(ΔG). As shown in Figure S5, Supporting Information, rms(ΔG) decreases when the analyzed voltage range is shifted to higher voltage due to the increasing current density in the NW. An estimation of the current length scale for the NWs yields $l_\mathrm{J} = 5 \times 10^{-9}$ nm, which is similar to l_ϕ explaining the decrease in rms(ΔG) with increasing current in agreement with previous results.[27] Thus, only considering the high voltage range (2) underestimates l_ϕ. The results demonstrate the necessity of only considering an intermediate voltage range for a reliable determination of l_ϕ.

Furthermore, l_ϕ shows only a weak temperature dependence below 30 K followed by a characteristic decrease with increasing temperature. The weak temperature dependence is in accordance with previous results obtained by magneto transport measurements at temperatures below 40 K.[25] As we observe UCFs at temperatures above 40 K, we are able to determine a characteristic temperature dependence of l_ϕ proportional to approximately $T^{-3/4}$ to T^{-1}, which indicates that electron–phonon scattering is the dominant dephasing mechanism at higher temperatures.[39,40]This allows the estimation of the electron–phonon scattering time $\tau_{e-\mathrm{Ph}}$:

$$l_\phi = \sqrt{D\tau_\phi} \approx \sqrt{D\tau_{e-\mathrm{Ph}}} \quad (3)$$

where D is the diffusion coefficient and τ_ϕ is the phase coherence time being comparable to $\tau_{e-\mathrm{Ph}}$ at higher temperatures. Using $l_\phi \approx 5$ nm and $D \approx 2\,\mathrm{cm^2\,Vs^{-1}}$ gives an electron–phonon scattering time of the order of 10^{-15} s, which is in excellent agreement with literature values reported for GaN.[25,41,42]

Typically, the UCFs of Ge-doped GaN NWs are examined using the magnetic field approach revealing a decrease of l_ϕ with decreasing doping concentration. However, UCFs have not been observed in non-intentionally doped GaN when applying a magnetic field.[25,27] Instead, the phase coherence length was determined solely from analyzing the weak localization effect giving comparable values of l_ϕ of about 10 nm. Thus, our results show that UCFs can arise even in non-intentionally doped GaN-NW–FET when shifting the Fermi level by applying a gate voltage and that the electric-field approach is a suitable approach to analyze mesoscopic transport properties of low-dimensional nanostructures.

4. Conclusion

In this work, we fabricated an FET based on a non-intentionally doped GaN NW. The FET turned out to be fully functional in the entire temperature range from room temperature down to 1.7 K. We identified UCFs at temperatures below 140 K arising due to the shift of the Fermi level and changes of the width of the conductive transport channel in the NW when applying a gate voltage. Both effects result in strong changes of the effective impurity concentration in the NW leading to the occurrence of UCFs. We analyzed the UCFs by determining the phase coherence length l_ϕ demonstrating that l_ϕ differs by a factor up to four depending on the chosen gate voltage range in which a value for l_ϕ is derived. This demonstrates that voltage-induced effects need to be considered when estimating l_ϕ from UCFs appearing in transfer characteristics. In addition, we were able to identify electron–phonon scattering as the phase-breaking mechanism at higher temperatures by determining the temperature dependence of l_ϕ. Our results show that the electrical field approach is more sensitive in case of non-intentionally doped GaN NWs to induce UCFs for determining the phase coherence length than the magnetic field approach.

Supporting Information

Supporting Information is available from the Wiley Online Library or from the author.

Acknowledgements

The authors gratefully acknowledge funding by the federal state of Hessen and the European Regional Development Fund. M.T.E. acknowledges financial support by the Heisenberg Program (project no. 498993886; grant no. EL 863/6-1) from the German Research Foundation (DFG). P.K. and S.C. gratefully acknowledge funding by the German Research Foundation (DFG) via the Collaborative Research Center no. 223848855-SFB 1083.

Open Access funding enabled and organized by Projekt DEAL.

Conflict of Interest

The authors declare no conflict of interest.

Data Availability Statement

The data that support the findings of this study are available from the corresponding author upon reasonable request.

Keywords

cryogenic temperatures, gallium nitride nanowire, mesoscopic transport properties, nanowire field-effect transistors, phase coherence length, universal conductance fluctuations

Received: January 12, 2024
Revised: February 9, 2024
Published online: March 3, 2024

[1] M. A. H. Khan, B. Thomson, J. Yu, R. Debnath, A. Motayed, M. V. Rao, *Sens. Actuators, B* **2020**, *318*, 128223.
[2] M. A. Johar, H. G. Song, A. Waseem, M. A. Hassan, I. V. Bagal, Y. H. Cho, S. W. Ryu, *Appl. Mater. Today* **2020**, *19*, 100541.

© 2024 The Authors. physica status solidi (a) applications and materials science published by Wiley-VCH GmbH

18626319, 2024, 21, Downloaded from https://onlinelibrary.wiley.com/doi/10.1002/pssa.202400040 by Justus-Liebig-Universitat, Wiley Online Library on [27/11/2024]. See the Terms and Conditions (https://onlinelibrary.wiley.com/terms-and-conditions) on Wiley Online Library for rules of use; OA articles are governed by the applicable Creative Commons License

[3] M. Behzadirad, S. Mecholdt, J. N. Randall, J. B. Ballard, J. Owen, A. K. Rishinaramangalam, A. Reum, T. Gotszalk, D. F. Feezell, I. W. Rangelow, T. Busani, *Nano Lett.* **2021**, *21*, 5493.
[4] K. Xie, J. Wang, S. Yu, P. Wang, C. Sun, *Arabian J. Chem.* **2021**, *14*, 103161.
[5] S. Mariana, J. Gülink, G. Hamdana, F. Yu, K. Strempel, H. Spende, N. Yulianto, T. Granz, J. D. Prades, E. Peiner, H. S. Wasisto, A. Waag, *ACS Appl. Nano Mater.* **2019**, *2*, 4133.
[6] M. A. H. Khan, R. Debnath, A. Motayed, M. V. Rao, *Sensors* **2021**, *21*, 624.
[7] M. F. Fatahilah, F. Yu, K. Strempel, F. Römer, D. Maradan, M. Meneghini, A. Bakin, F. Hohls, H. W. Schumacher, B. Witzigmann, A. Waag, H. S. Wasisto, *Sci. Rep.* **2019**, *9*, 10301.
[8] L. Liu, F. Lu, J. Tian, *Appl. Surf. Sci.* **2020**, *508*, 145250.
[9] O. Lupan, G. Chai, L. Chow, G. A. Emelchenko, H. Heinrich, V. V. Ursaki, A. N. Gruzintsev, I. M. Tiginyanu, A. N. Redkin, *Phys. Status Solidi A* **2010**, *207*, 1735.
[10] E. Barrigón, M. Heurlin, Z. Bi, B. Monemar, L. Samuelson, *Chem. Rev.* **2019**, *119*, 9170.
[11] Y. Huang, X. Duan, Y. Cui, C. M. Lieber, *Nano Lett.* **2002**, *2*, 101.
[12] G. Suo, S. Jiang, J. Zhang, J. Li, M. He, *Adv. Condens. Matter Phys.* **2014**, *2014*, 456163.
[13] J. Sim, K. Kim, S. Song, J. Kim, *Analyst* **2013**, *138*, 2432.
[14] C. Zhao, T. K. Ng, R. T. Elafandy, A. Prabaswara, G. B. Consiglio, I. A. Ajia, I. S. Roqan, B. Janjua, C. Shen, J. Eid, A. Y. Alyamani, M. M. El-Desouki, B. S. Ooi, *Nano Lett.* **2016**, *16*, 4616.
[15] L. Nela, J. Ma, C. Erine, P. Xiang, T. H. Shen, V. Tileli, T. Wang, K. Cheng, E. Matioli, *Nat. Electron.* **2021**, *4*, 284.
[16] S. Singh, A. Raman, *Silicon* **2020**, *14*, 1297.
[17] M. Zhou, H. Qiu, T. He, J. Zhang, W. Yang, S. Lu, L. Bian, Y. Zhao, *Phys. Status Solidi A* **2020**, *217*, 2000061.
[18] A. L. Bavencove, G. Tourbot, E. Pougeoise, J. Garcia, P. Gilet, F. Levy, B. André, G. Feuillet, B. Gayral, B. Daudin, L. S. Dang, *Phys. Status Solidi A* **2010**, *207*, 1425.
[19] Y. Kurisaki, S. Kamiyama, M. Iwaya, T. Takeuchi, I. Akasaki, *Phys. Status Solidi A* **2017**, *214*, 1600867.
[20] D. J. Carter, J. D. Gale, B. Delley, C. Stampfl, *Phys. Rev. B* **2008**, *77*, 115349.
[21] G. Santoruvo, A. Allain, D. Ovchinnikov, E. Matioli, *Appl. Phys. Lett.* **2016**, *109*, 103102.
[22] P. Y. Yang, L. Y. Wang, Y. W. Hsu, J. J. Lin, *Phys. Rev. B* **2012**, *85*, 085423.
[23] T. E. Park, B. C. Min, J. Lee, J. Jeon, K. Y. Lee, H. J. Choi, J. Chang, *Nanotechnology* **2020**, *32*, 125702.
[24] P. A. Lee, A. D. Stone, H. Fukuyama, *Phys. Rev. B* **1987**, *35*, 1039.
[25] M. T. Elm, P. Uredat, J. Binder, L. Ostheim, M. Schäfer, P. Hille, J. Müßener, J. Schörmann, M. Eickhoff, P. J. Klar, *Nano Lett.* **2015**, *15*, 7822.
[26] J. J. Lin, J. P. Bird, *J. Phys.: Condens. Matter* **2002**, *14*, 501.
[27] P. Uredat, P. Hille, J. Schörmann, M. Eickhoff, P. J. Klar, M. T. Elm, *Phys. Rev. B* **2019**, *100*, 085409.
[28] A. S. Lien, L. Y. Wang, C. S. Chu, J. J. Lin, *Phys. Rev. B* **2011**, *84*, 155432.
[29] S. Alagha, S. E. Hernández, C. Blömers, T. Stoica, R. Calarco, T. Schäpers, *J. Appl. Phys.* **2010**, *108*, 113704.
[30] J. Kim, S. Lee, Y. M. Brovman, M. Kim, P. Kim, W. Lee, *Appl. Phys. Lett.* **2014**, *104*, 043105.
[31] J. Schörmann, P. Hille, M. Schäfer, J. Müßener, P. Becker, P. J. Klar, M. Kleine-Boymann, M. Rohnke, M. De La Mata, J. Arbiol, D. M. Hofmann, J. Teubert, M. Eickhoff, *J. Appl. Phys.* **2013**, *114*, 103505.
[32] M. Schäfer, M. Günther, C. Länger, J. Müßener, M. Feneberg, P. Uredat, M. T. Elm, P. Hille, J. Schörmann, J. Teubert, T. Henning, P. J. Klar, M. Eickhoff, *Nanotechnology* **2015**, *26*, 135704.
[33] J. W. Yu, C. K. Li, C. Y. Chen, Y. R. Wu, L. J. Chou, L. H. Peng, *Appl. Phys. Lett.* **2011**, *99*, 152108.
[34] S. M. Sze, K. K. Ng, *Physics Of Semiconductor Devices*, Wiley-Interscience, Hoboken, NJ **2007**.
[35] B. S. Simpkins, M. A. Mastro, C. R. Eddy, P. E. Pehrsson, *J. Appl. Phys.* **2008**, *103*, 104313.
[36] C. W. J. Beenakker, H. Van Houten, *Solid State Phys.* **1991**, *44*, 1.
[37] S. Estévez Hernández, M. Akabori, K. Sladek, C. Volk, S. Alagha, H. Hardtdegen, M. G. Pala, N. Demarina, D. Grützmacher, T. Schäpers, *Phys. Rev. B* **2010**, *82*, 235303.
[38] C. W. J. Beenakker, H. Van Houten, *Phys. Rev. B* **1988**, *37*, 6544.
[39] N. Giordano, *Phys. Rev. B* **1980**, *22*, 5635.
[40] H. Fukuyama, E. Abrahams, *Phys. Rev. B* **1983**, *27*, 5976.
[41] V. P. Zhukov, V. G. Tyuterev, E. V. Chulkov, P. M. Echenique, *J. Appl. Phys.* **2016**, *120*, 085708.
[42] K. T. Tsen, D. K. Ferry, A. Botchkarev, B. Sverdlov, A. Salvador, H. Morkoç, *J. Appl. Phys.* **1997**, *71*, 1852.

© 2024 The Authors. physica status solidi (a) applications and materials science published by Wiley-VCH GmbH

18626319, 2024, 21, Downloaded from https://onlinelibrary.wiley.com/doi/10.1002/pssa.202400040 by Justus-Liebig-Universitat, Wiley Online Library on [27/11/2024]. See the Terms and Conditions (https://onlinelibrary.wiley.com/terms-and-conditions) on Wiley Online Library for rules of use; OA articles are governed by the applicable Creative Commons License